# Production cross-section and reaction yield calculations for $^{123-126}$I isotopes on $^{123}$Sb(α,xn) reactions

Hasan Özdoğan[1,2], Mert Şekerci[3], Abdullah Kaplan[3,*]

[1]*Dept. of Biophysics, Akdeniz University, 07070, Antalya, Turkey*
[2]*Dept. of Medical Imaging Techniques, Vocational School of Health Services, Antalya Bilim University, 07190, Antalya, Turkey*
[3]*Dept. of Physics, Süleyman Demirel University, 32260, Isparta, Turkey*
*Corresponding author: abdullahkaplan@sdu.edu.tr*

## Abstract

Most of the radioisotopes used in the medical fields, like examination and treatment studies, were produced by employing nuclear reactions. Within the process of a nuclear reaction, one of the most important parameters is the cross-section data, which help reveal the reaction phenomenon's mechanisms. The main intention of this study is to investigate the efficiencies of producing iodine isotopes via $^{123}$Sb(α,xn) reactions. For this, optical and level density models of TALYS 1.8 code have been used. Production cross-section, the alpha beam energy, reaction yields, and total activation of radioisotopes have been computed. It has been figured out that a 45 MeV cyclotron could be enough for producing $^{123-126}$I radioisotopes with reaction yields of 39.3372, 5.5685, 0.2410, and 0.0796 GBq/mAh, respectively.

**Keywords:** Alpha-induced; cross-section; production of iodine isotopes; reaction yield; TALYS code.

## 1. Introduction

There exist numerous radioisotopes utilized for medicinal examinations and treatments. An extensively used example among them could be given as the isotopes of iodine. $^{123}$I, probably the most widely used cyclotron generated radiohalogen, has gradually taken over the spot of $^{131}$I for the diagnostic radiopharmaceuticals containing radio iodine. A distinguishing reason to prefer $^{123}$I is based on its lower radiation dose. Another one could be pointed to as the 159 keV gamma-ray energy, which optimally fits the use in gamma cameras (IAEA-TECDOC 468, 2009). The most common method for producing $^{123}$I is $^{124}$Te(p,2n) reaction. $^{124}$I with 4.2 days of half-life is used for PET imaging of monoclonal antibodies. Generally, $^{124}$I is produced by $^{124}$Te(p,n) reaction. On the other hand, with 59.4 days of half-life and lower gamma emission, a functional radioisotope $^{125}$I has to gain widespread usage, especially in diagnostic and therapeutic applications. Also, it is known that recent applications employ in vitro diagnostic kits (radioimmunoassays) for bone dosimetry devices, protein ionization, and therapeutic seed implants for prostate cancer treatment.

The cross-section of a nuclear reaction, which is often called the excitation function, represents the amount of total probability of the primary generation of a compound nucleus and secondly, decaying along a

particular channel. Not only the amount of a radionuclide that is aimed to be produced within a cyclotron but also the levels of contamination due to the other radioisotopes that exist in the target could be determined by using the cross-section values. Due to that, reaction cross-section knowledge is crucial to obtain maximum radioisotope impurities. Level density and optical models have a key role in accurately calculating cross-section data (Özdoğan, 2019; Yiğit, 2018; Voinov *et al.,* 2014).

The main aim of this study is to investigate the efficiencies of producing iodine isotopes via alpha-induced reactions. The first part of this study has been constructed to obtain the reaction cross section values based on alpha optical models to reach our aim. The best alpha optical models for each investigated reaction with respect to experimental data, which have been taken from Experimental Nuclear Reaction Data (EXFOR) (EXFOR, 2020) library, have been determined by using a relative variance analysis method (Kurenkov *et al.,* 1999). After obtaining the best optical models for each reaction route, cross-section calculations have been redone using the level density models to fix the obtained best optical models. Relative variance analysis has been done again to be able to appoint the best level density model in each reaction route. In addition to the theoretical reaction cross-section calculations, alpha beam energies for each reaction route have been determined using appointing the energy values where the reaction cross-section data have obtained in the maximum level with the employment of the best models. As one of the investigated property within this study, reaction yield and total activation values of radioisotopes have been calculated for 10 hours of irradiation with alpha particles. All calculations have been performed by using TALYS 1.8 (Koning *et al.,* 2015) code.

## 2. Materials and Methods

Many techniques, such as theoretical and experimental studies, are employed within scientific investigations to answer the phenomenon of nature. Computational analyzation and simulation studies are very useful to answer the questions when the experimental data are absent. Simulations can be applied in many areas, from physics to chemistry and clinical sciences (Locharoenrat, 2020; Sumaryada *et al.,* 2019; Mahdavian, 2017; Singh *et al.,* 2017; Sadeghi *et al.,* 2010; Belgaid & Muhammad, 2003).

Like many branches of physics, various computer codes could be utilized in theoretical nuclear physics. The most known and preferred one among them is the TALYS code that can run under the Unix operating systems. With the new versions of the TALYS code, it is possible to investigate proton, neutron, deuteron, triton, $^{3}$He, $^{4}$He, and photon-induced reactions up to 1000 MeV projectile energy. In this study, all calculations have been completed by using a computer with Intel Core I7 CPU 2.6 GHZ processor endowed with 32 GB RAM in where a Linux operation system is running. In accordance with the purpose of this study, the 1.8 version of the TALYS code has been employed for the calculations in where various level density models and alpha optical model potentials have been utilized.

As a result of the long-term development studies of the nuclear level density models, sophisticated microscopic models were generated, but phenomenological models still have great importance. The basic level density model could be pointed to as Fermi Gas Model (FGM), which was also used to derive other phenomenological models.

In the assumption of this model, protons and neutrons occupy the lowest energy states, and in the case of excitation, they fill

higher ones. This assumption provides successful results to FGM for low energies but fails with the increase of energy. This situation has been resolved by adopting a constant temperature approach in where the model was named as Constant Temperature Fermi Gas Model (CTFGM) and divided the energy region into two sections as low and high. Within the concept of CTFGM, the constant temperature law is valid in the energy range from 0 MeV to the matching energies, while FGM is valid in the energies which are higher than the matching energy (Ignatyuk *et al.*, 1979). Following the development of this model, a new approach has been represented as the Back Shifted Fermi Gas Model (BSFGM), where the pairing energy has been treated as an arrangeable parameter, and the FGM was applied to the all lower energies down to 0 MeV (Baba, 1970).

In addition to the mentioned level density models, one more model named as Generalised Superfluid Model (GSM) has been employed in this study which was characterized by a phase transition from the low-energy super-fluid behaviour, where the superconductivity correlations exist according to the Bardeen Cooper-Schrieffer theory, to the high-energy region defined by the Fermi Gas Model (Ignatyuk *et al.*, 1975).

Besides the investigations of level density models, the effects of optical model parameters were also examined in this study. The optical model's fundamental hypothesis is related to the complicated interactions between an incident particle and a nucleus where it is possible to represent it by a complex mean-field potential, which divides the reaction flux into a part covering shape elastic scattering and a part describing all competing non-elastic channels. Generally, alpha optical potentials are focused on potential wells with a depth of 50 MeV. However, McFadden & Satchler though that alpha optical potential is a superposition of four nucleon nucleus potentials that has a depth of 200 MeV (McFadden & Satchler, 1966). Besides the McFadden & Satchler optical potential, TALYS has different optical potentials for alpha particles, such as Watanabe folding approach Koning Delaroche (Watanabe, 1958), Demetriou Grama-Goriely (Demetriou *et al.*, 2002), and Avrigeanu (Avrigeanu & Avrigeanu, 2010) optical potentials, which were used in this paper.

## 3. Results and Discussion

In this study, the production cross-sections, reaction yields, and total activities of $^{123\text{-}126}$I isotopes were investigated by employing both level density and alpha optical models via TALYS 1.8 code. The obtained production cross-section calculations were represented in Figures 1 and 2. By using these computation results and relative variance analysis, which were given in Tables 1 and 2, the most convenient alpha optical and level density models were determined for each reaction route. This process led us to have the required data to obtain the reaction yields and total activation results, which were given in Figures 3-10.

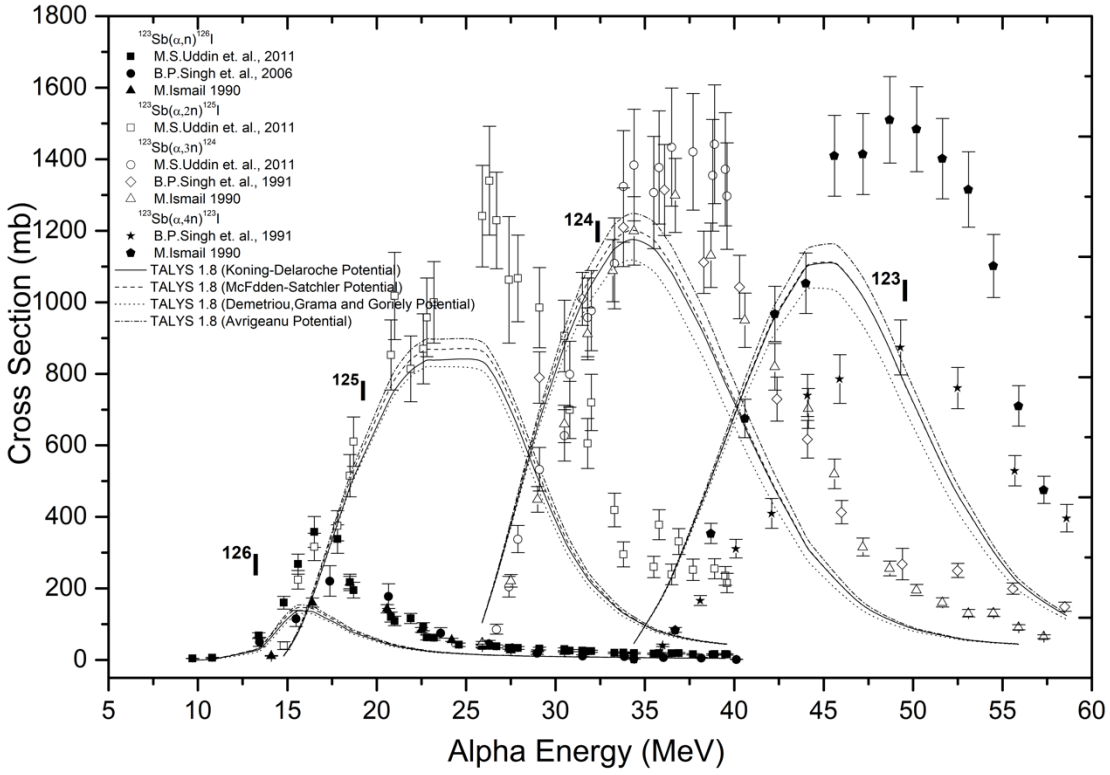


**Fig. 1.** Reaction cross-section calculations with alpha optical models.

In Figure 1, comparisons of $^{123}Sb(\alpha,n)^{126}I$ cross-section calculations with experimental data of Uddin *et al.,* 2011; Singh *et al.,* 2006; and Ismail, 1990, were given. All calculations were in good agreement with the experimental data up to 17 MeV. According to the statistical analysis given in Table 1, the Avrigeanu optical model could be considered the most successful model for this reaction.

$^{123}Sb(\alpha,2n)^{125}I$ reaction cross-section calculations against the experimental data of Uddin *et al.,* 2011, were also shown in Figure. 1. All calculations based on different alpha optical models were consistent with the EXFOR data up to 23 MeV, where the Avrigeanu optical model was found as the best model as a result of relative variance analysis.

Obtained $^{123}Sb(\alpha,3n)^{124}I$ reaction cross section calculations were compared with the experimental data taken from the experimental studies of Uddin *et al.,* 2011; Singh *et al.,* 1991; and Ismail, 1990, where the outcomes were given in Figure. 1. All calculations were well matched with the experimental data except the energy region beyond 37 MeV. Avrigeanu optical model is the best model, according to Table 1.

$^{123}Sb(\alpha,4n)^{123}I$ reaction cross-section calculations against the experimental data of Singh *et al.,* 1991; and Ismail, 1990, were also presented in Figure.1. As can be clearly seen from the figure, experimental data exhibit an obvious discrepancy from each other. According to the relative variance analysis, Demetriou, Grama, Goriely optical model is the best option for this reaction.

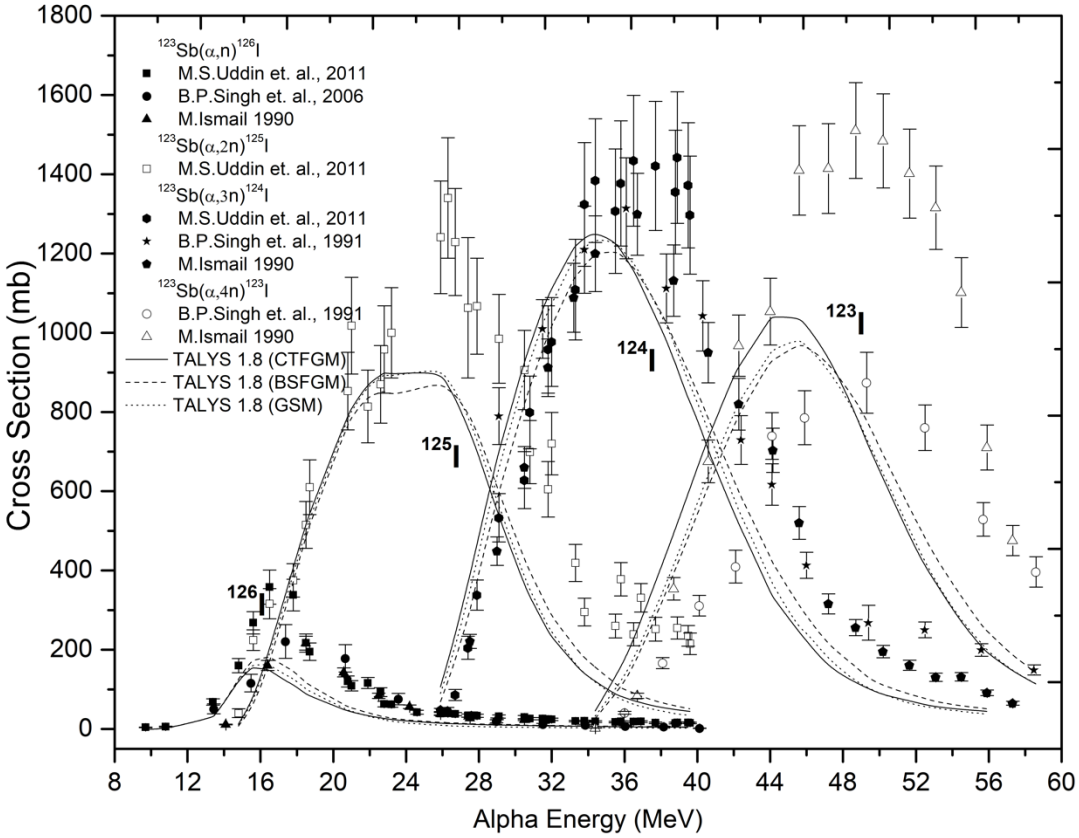


**Fig. 2.** Reaction cross-section calculations with level density models.

Production cross-sections were recalculated by using the best alpha optical models through the different level density models. Comparisons of theoretical calculations with the experimental data were given in Figure. 2.

For $^{123}Sb(\alpha,n)^{126}I$cross–section calculations, which were presented in Figure 2. Avrigeanu was the appointed optical model. As shown in Table 2., BSFGM is the best level density option for this reaction. According to the best model, the maximum cross-section was obtained as 182.271 mb at 16.4 MeV alpha particle energy. Therefore, the optimum beam energy to produce $^{126}I$ was appointed as 16.4 MeV.

$^{123}Sb(\alpha,2n)^{125}I$ cross-section calculations through the phenomenological level density models were also shown in Figure 2. The selected alpha optical model for this reaction was Avrigeanu potential, and this can be seen from the relative variance analysis given in Table 2. BSFGM could be given as the most convenient model with respect to the experimental data. The maximum cross section value is 877.633 mb at 25.9 MeV, which is also selected as the alpha particle beam energy.

Production cross–section calculations of $^{124}I$ through the (α,3n) reaction were presented in Figure. 2. Generally, all level density model results are obtained as close to each other. According to the relative variance analysis, BSFGM was the best level density model. The peak cross-section value, which is 1204.81 mb, was obtained at 35.5 MeV alpha energy. Considering this, the beam energy for $^{124}I$ was selected as 35.5 MeV.

For the $^{123}Sb(\alpha,4n)^{123}I$ reaction cross section calculations versus alpha energy, shown in Figure 2, BSFGM was found to be the best-level density model. The maximum cross-section value based on BSFGM calculation is 972.141 mb at 45.6 MeV. Therefore, the beam energy was selected as 45.6 MeV.

One of the most important parts of the radioisotope production procedure could be separating the radioisotope from the target material. The information of reaction yield gives the ratios of different isotope production results of a nuclear reaction and therefore has undeniable importance. The obtained reaction yield calculations within the scope of this study were presented in Figures 3-6.

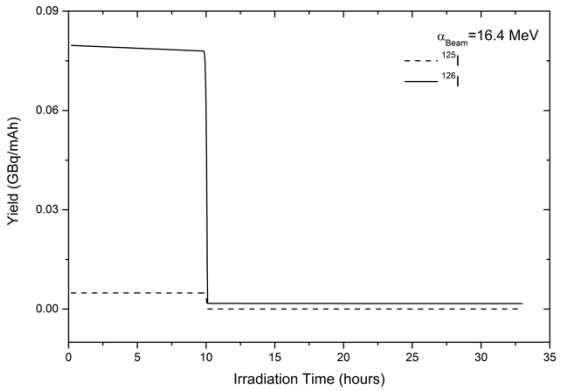


**Fig. 3.** Reaction yield calculations via 16.4 MeV alpha beam.

At 16.4 MeV alpha beam energy, clearly seen in Figure. 3, $^{125,126}I$ reaction yields are 0.0048 and 0.0796 GBq/mAh, respectively. In other words, $^{126}I$ production is 16.3 times larger than $^{125}I$ in this particular situation.

In Figure 4, reaction yield results at 25.9 MeV beam energy versus irradiation time were given. $^{124\text{-}126}I$ radioisotopes could be obtained after irradiation of 25.9 MeV alpha particles. Reaction yields of $^{124\text{-}126}I$ radioisotopes are 0.0797, 0.2410, and 0.0399 GBq/mAh, respectively.

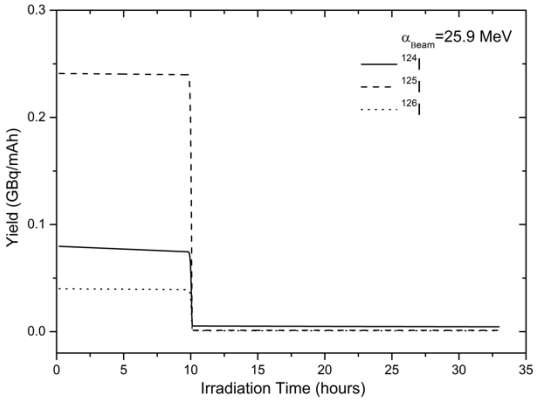


**Fig. 4.** Reaction yield calculations via 25.9 MeV alpha beam.

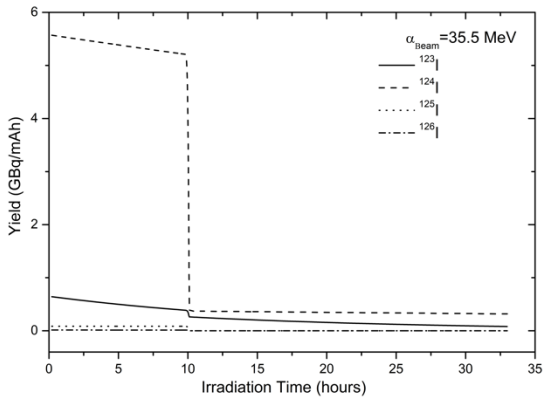


**Fig. 5.** Reaction yield calculations via 35.5 MeV alpha beam.

Irradiation of 35.5 MeV alpha beam reaction yield results was presented in Figure 5. As shown in this figure, $^{123\text{-}126}I$ radioisotopes were obtained after the bombarding process with the reaction yields of 0.6403, 5.5685, 0.0857, and 0.0141 GBq/mAh, respectively.

In Figure 6, reaction yield results at 45.6 MeV were shown. $^{123\text{-}126}I$ radioisotopes were produced after irradiation, where the reaction yields of $^{123\text{-}126}I$ have been obtained as 39.3372, 2.7145, 0.0159, and 0.0082 GBq/mAh, respectively.

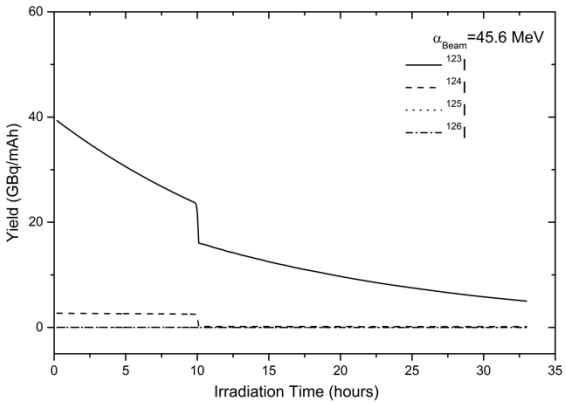


**Fig. 6.** Reaction yield calculations via 45.6 MeV alpha beam.

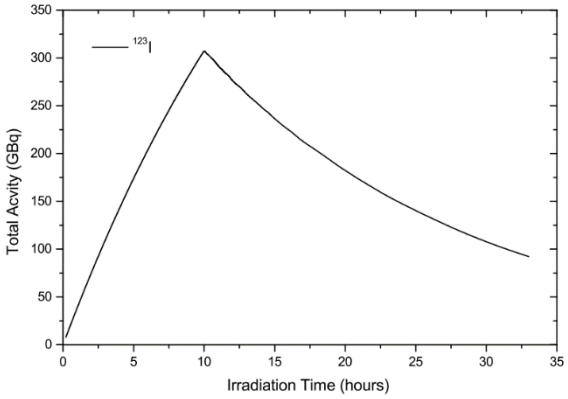


**Fig. 7.** Total activity of $^{123}$I.

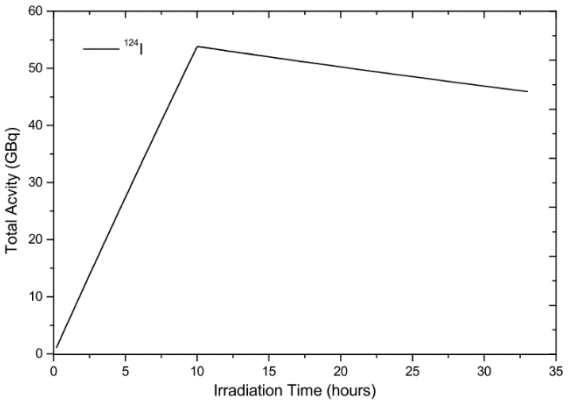


**Fig. 8.** Total activity of $^{124}$I.

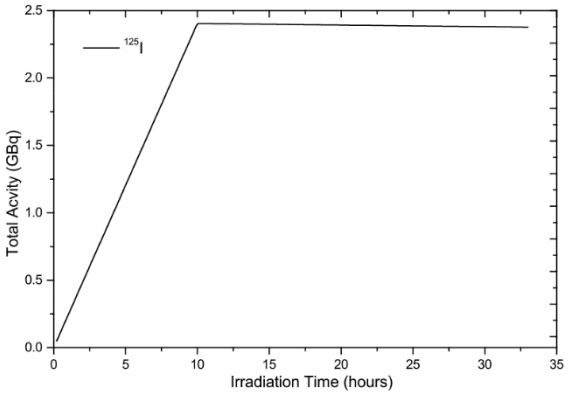


**Fig. 9.** Total activity of $^{125}$I.

Total activation calculations versus irradiation time were presented in Figures 7-10. For each radioisotope, the beam energy was selected to obtain the maximum yield. The maximum total activities for $^{123\text{-}126}$I radioisotopes are 307.1320, 53.8360, 2.4042, and 0.7878 GBq, respectively. Total activities are constant up to half-life periods after cutting of the irradiation.

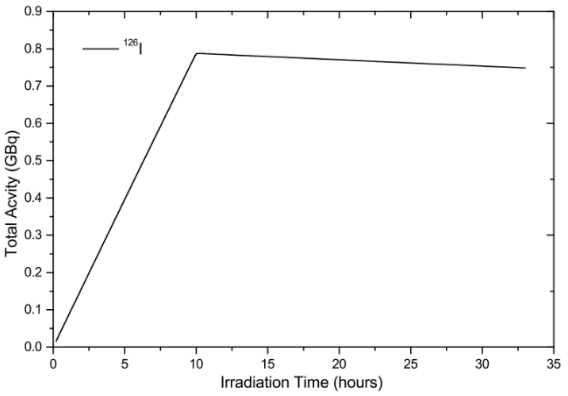


**Fig. 10.** Total activity of $^{126}$I.

**Table 1.** Relative variance analysis of production cross–section calculations by using alpha optical models.

| Radioisotope | Koning-Delaroche Potential | McFadden-Satchler Potential | Demetriou, Grama and Goriely Potential | Avrigeanu Potential |
|---|---|---|---|---|
| $^{123}$I | 1.3821 | 1.3888 | 1.3774 | 1.3965 |
| $^{124}$I | 0.3908 | 0.3948 | 0.4114 | 0.3853 |
| $^{125}$I | 0.4675 | 0.4536 | 0.4838 | 0.4408 |
| $^{126}$I | 0.6581 | 0.6599 | 0.6611 | 0.6580 |

**Table 2.** Relative variance analysis of production cross–section calculations by using level density models.

| Radioisotope | CTFGM | BSFGM | GSM |
|---|---|---|---|
| $^{123}$I | 1.3774 | 0.9049 | 1.0661 |
| $^{124}$I | 0.3853 | 0.2690 | 0.3430 |
| $^{125}$I | 0.4480 | 0.4196 | 0.4470 |
| $^{126}$I | 0.6580 | 0.6119 | 0.7734 |

## 4. Conclusion

In this paper, radioisotope production cross-section calculations of $^{123-126}$I from $^{123}$Sb(α,xn) reactions have been studied.

Also, reaction yields and total activities of radioisotopes have been calculated. Obtained results can be summarized as follows:

- All-optical and level density model calculations give similar results to each other.
- Avrigeanu optical model could be pointed out as the best optical model option except than the (α,4n) reaction. This model's parameters can be used for future investigations of $^{123}$Sb targeted nuclear reactions.
- BSFGM is the most successful level density model for the reaction routes that were examined in this study.
- Alpha beam energies to obtain $^{123-126}$I isotopes were obtained as 45.6, 35.5, 25.9, and 16.4 MeV, with respect to the order of the isotopes. As can be seen, an alpha beam of approximately 45 MeV

could be sufficient to obtain iodine radioisotopes via the investigated reaction routes in this paper. $^{123-125}$I can be obtained by proton-induced nuclear reactions at 30 MeV (Hohn *et al.*, 2001). This paper also indicates that the reaction yields of total activations for $^{123-126}$I radioisotopes on alpha-induced reactions.

- Similar works should be performed for a better understanding of radioisotope production studies via proton-induced reactions.
- Maximum activities of $^{123-126}$I radioisotopes after the irradiations were found as 307.1320, 53.8360, 2.4042, and 0.7878 GBq, respectively.
- The maximum reaction yields were determined as 39.3372, 5.5685, 0.2410, and 0.0796 GBq/mAh for $^{123-126}$I radioisotopes, respectively.

## References

**Avrigeanu, M. & Avrigeanu, V. (2010)** α-particle nuclear surface absorption below the Coulomb barrier in heavy nuclei. Phys. Rev. C. **82**, 1-7.

**Baba, H. (1970)** A shell-model nuclear level density. Nucl. Phys. A. **159**, 625–641.

**Belgaid, M.; Muhammad, A. (2003)** Semi-empirical systematics of (n, He-3) cross-sections for 14.6 MeV neutrons. Nucl. Instrum. Methods Phys. Res., B. **201**, 463-472.

**Demetriou, P.; Grama, C.; Goriely, S. (2002)** Improved global α-optical model potentials at low energies. Nucl. Phys. A. **707**, 253-276.

**EXFOR. (2020)** (Experimental Nuclear Reaction Data File), Brookhaven National Laboratory, National Nuclear Data Center, Database Version of **2020-03-02**.

**Hohn, A.; Nortier, F. M.; Scholten, B.; van der Walt, T. N.; Coenen, H. H *et al.* (2001)** Excitation functions of $^{125}$Te(p,xn)-reactions from their respective thresholds up to 100 MeV with special reference to the production of $^{124}$I, App. Rad. Isot. **55**, 149-156.

**IAEA-TECDOC-468. (2009)** Cyclotron Produced Radionuclides: Physical Characteristics and Production Methods Technical. Vienna IAEA.

**Ignatyuk, A. V.; Smirenkin, G. N.; Tishin, A. S. (1975)** Phenomenological description of the energy dependence of the level density parameter. Sov. J. Nucl. Phys. **21**, 255.

**Ignatyuk, A. V.; Istekov, K. K.; Smirenkin, G. N. (1979)** The role of collective effects in the systematics of nuclear level densities. Yad. Fiz. **29**, 875–883.

**Ismail, M. (1990)** Measurement and analysis of the excitation function for alpha-induced reactions on Ga and Sb isotopes. Phys. Rev. C. **41**, 87-108.

**Koning, A.; Hilaire, S.; Goriely, S. (2015)** TALYS–1.8 A Nuclear Reaction Program, User Manual, 1st ed. NRG, The Netherlands.

**Kurenkov, N. V.; Luneva, V. P.; Shubina, Yu. N. (1999)** Evaluation of calculation methods for excitation functions for production of radioisotopes of iodine, thallium, and other elements. Appl. Radiat. Isot. **50**, 541–549.

**Locharoenrat, K. (2020)** Computational algorithm of high-intensity focused ultrasound beam of cancer tissue model for hyperthermia therapy. Kuwait J. Sci. Eng. **47**, 50-64.

**Mahdavian, L. (2017)** Simulation and calculation of 2, 4, 5, 2′, 4′, 5′ - hexachlorobiphenyl passing from the central axis of single-walled carbon nanotube. Kuwait J. Sci. Eng. **44**, 97-104.

**McFadden, L. & Satchler, G. R. (1966)** Optical model analysis of the scattering of

24.7 MeV alpha particles. Nucl. Phys. **84**, 177-200.

**Özdoğan, H. (2019)** Theoretical calculations of production cross-sections for the $^{201}$Pb, 111In, 18F, and 11C radioisotopes at proton-induced reactions. Appl. Radiat. Isot. **143**, 1-5.

**Sadeghi, M.; Kakavand, T.; Alipoo, Z. (2010)** $^{85}$Sr Production via proton-induced on various targets using Talys 1.0 code. Mod. Phys. Lett. A. **25**, 1541-1552.

**Singh, B. P.; Bhardwaj, H. D.; Prasad, R. (1991)** A study of pre-equilibrium emission in α-induced reactions on $^{121,123}$Sb. Can. J. Phys., **69**, 1376-1.

**Singh, B. P.; Sharma, M. K.; Musthafa, M. M.; Bhardwaj, H. D.; Prasad, R. (2006)** A study of pre-equilibrium emission in some proton and alpha-induced reactions. Nucl. Instrum. Methods in Physics Res., Sect.A. **562**, 717-720.

**Singh, B.; Singh, R.; Singh, B.; Kumar, D. (2017)** Computational study on molecular structure, vibrational and electronic properties of a novel Schiff base: Benzyl2-(4-(bis(2-cloroethyl) benzylidene) hydrazinecarbodithioate. Kuwait J. Sci. Eng. **44**, 98-109.

**Sumaryada, T.; Sofyan, A.; Syafutra, H. (2019)** Simulation of the extra-terrestrial and terrestrial performance of GaAs/Ge dual-junction solar cells. Kuwait J. Sci. Eng. **46**, 58-65.

**Uddin, M. S.; Hermanne, A.; Sudár, S.; Aslam, M. N.; Scholten, B *et al.* (2011)** Excitation functions of α-particle induced reactions on enriched $^{123}$Sb and $^{nat}$Sb for production of $^{124}$I. Appl. Radiat. Isot. **69**, 699-704.

**Voinov, A. V.; Grimes, S. M.; Brune, C. R.; Bürger, A.; Görgen, A *et al.* (2014)** Level density inputs in nuclear reaction codes and role of the spin cutoff parameter. Nucl. Data Sheets, **119**, 255-257.

**Watanabe, S. (1958)** High energy scattering of deuterons by complex nuclei. Nucl. Phys. **8**, 84-492.

**Yiğit, M. (2018)** A review of (n,p) and (n, a) nuclear cross-sections on palladium nuclei using different level density models and empirical formulas. Appl. Radiat. Isot. **140**, 355-362.

**Submitted** : 04/03/2020

**Revised** : 14/07/2020

**Accepted** : 26/07/2020

**DOI** : 10.48129/kjs.v48i2.9310